Transpiration through hydrogels

Supplementary Material

Merlin A. Etzold[1]†, Paul. F. Linden[1] and M. Grae Worster[1]

[1]Department of Applied Mathematics and Theoretical Physics, Centre for Mathematical Sciences, University of Cambridge, Wilberforce Road, Cambridge, CB3 0WA, UK

The supplementary material contains additional experimental details and the additional, time-resolved datasets which were used to compile the steady state graph shown in figure 10. The included datasets are summarised in table iii. Table iv provides the numerical data associated with the arrows in the time-resolved datasets.

1. Additional experimental details

1.1. *Materials*

We used commercially available polyacrylamide hydrogel beads intended as soil moisturisers (Soilmoist, *JRM Chemicals*, 4881 NEO Parkway, Cleveland, Ohio 44128, US). On request, JRM Chemicals confirmed the hydrogel to be a poly(acrylamide potassium acrylate)copolymer, where the acrylate groups carry a negative charge and potassium is the counterion. JRM Chemicals also confirmed that, before 2018, their hydrogel beads with a dry diameter of less than 3.05 mm where obtained from a single-vat process by sieving.

Our beads were selected from the 1.5 mm to 2 mm (dry) sieve fraction, which can swell up to 14 mm in diameter. The Young's modulus of beads from different sieve fractions has been reported to be around 20 kPa for beads from a smaller sieve fraction (MacMinn *et al.* 2015), and to be between 12 and 27 kPa (average: approximately 16 kPa) by Zhang *et al.* (2021) for beads from a larger sieve fraction obtained at the same time as the beads used in this work. The latter indicates that the properties of individual beads may vary considerably. The beads used in any given experiment were chosen to be approximately of the same saturated size.

We characterised the variability of the properties of individual beads by measuring dry and wet sizes of 20 randomly chosen beads after five days of swelling. The results are collated in table i.

The maximum and minimum values for the dry diameter d_d are consistent with the chosen sieve fraction (1.5 mm to 2 mm). Nevertheless, the sample average particle size has only a small standard deviation of 4.1 %. This could be a property of the manufacturing process or due to size stratification of the beads in the storage bag. The standard deviation found for the average swollen bead size d_0 is comparable to that of the dry particle size. This indicates that the swelling properties are remarkably constant. This is confirmed by the small standard deviations of d_0/d_d and ϕ_0.

We observed that the final size of beads equilibrated with liquid water depends strongly on the presence of (ionic) species in the water. This suggests that ionic effects strongly contribute to the swelling. For example, even low sodium chloride or potassium carbonate concentrations lead to reduced equilibrium sizes and higher concentrations to no swelling

† Email address for correspondence: merlinaetzold@cantab.net

	Minimum	[mm] Average	Maximum
d_d	1.6	$1.86 \pm 4.1\,\%$	1.94
d_0	9.98	$11.45 \pm 3.9\,\%$	12.01
d_0/d_d	5.94	$6.15 \pm 1.9\,\%$	6.39
ϕ_0	3.83 ‰	$4.31\,‰ \pm 5.6\,\%$	4.77 ‰

Table i: Dry diameter, swollen diameter (first swelling, after 5 d), relative change in diameter and swollen volume fraction for 20 randomly chosen hydrogel beads. The average is characterised by its standard deviation.

Salt	$\approx \mathcal{RH}$	Salt	$\approx \mathcal{RH}$
potassium carbonate	0.43	magnesium nitrate	0.54
Potassium acetate	0.23	potassium chloride	0.85
sodium chloride	0.75	potassium nitrite	0.65†

Table ii: Overview of saturated salt solutions used for humidity control and expected relative humidity values at 22 °C (Greenspan 1977). † - from www.engineeringtoolbox.com

at all. We, therefore, chose to swell our beads in ultra-pure water (biological medium grade) to avoid any ionic effects.

Salt solutions for relative humidity controls were made by mixing an excess of the appropriate salt (a full list is given in table ii) with deionised water and left overnight.

1.2. *Sensors and data logging*

A *Nikon (Japan)* D5000 camera with a *Nikon* 105mm f2.8 G AF-S VR IF ED Micro Nikkor lens was mounted approximately 50 cm above the bead holders to monitor the bead size. We usually recorded three pictures per hour, sometimes up to twelve.

We measured the relative humidity and temperature of the air before and after the chamber of the bead with *Sensirion (Switzerland)* SHT-31D combined humidity-temperature sensors on *Adafruit (United Kingdom)* breakout boards, a third SHT-31D is used to monitor the environmental conditions. The flow was measured with an *Omega Engineering* FMT-1700/1800 series digital flow meter apart from one dataset, where a rotameter after the evaporation chamber was used instead. In some experiments, we used a second aquarium pump to mix the air in the evaporation chamber with a nominal rate of 3.5 l/ min.

The offset between the humidity sensors was determined by purging an empty setup with air from a given salt solution, which specifies the humidity of this air (Greenspan 1977). After the readings of the sensors had reached constant value the offset between the sensors was recorded. A linear interpolation method was then used to find the offset for sensor readings between the calibration points. Note that this does not affect the error of the absolute reading which remains $\pm 2\,\% - \mathcal{RH}$ as stated by the manufacturer, which is the accuracy of the absolute values for $\mathcal{RH}_i$ in table iv.

The air flow sensors were calibrated against a QM1 Rotameter (60-600 cc/min, G.A. Platon Ltd, Basingstoke, UK) since different sensors were found to have offsets between $\pm 0.15\,\mathrm{l\,min^{-1}}$.

A Raspberry Pi 3B was used for camera control and data logging together with a TCA9548A (*Texas Instrumens, US*) i2c multiplexer (for interfacing multiple SHT-31D) and a ADS1115 (*Texas Instruments*) analogue-digital converter for interfacing the flow rate sensors.

1.3. *Data processing*

An example image taken by the camera is shown in figure 1. In the upright state they appear much darker than the environment (bottom row) or slightly brighter with a dark region. The dark region is caused by the projection of the darker hole of the bead holder onto the bead surface; the beads actually remained clear.

The Scikit-Image library (van der Walt *et al.* 2014) was used for image processing. A Canny Edge detector was used to find the edges of the ellipsoids. Since the beads are transparent, the intensity gradient at the bead edge for those beads appearing clear was of comparable magnitude to intensity variations caused by reflections from the bead surface and inhomogeneous illumination. Therefore, suitable Canny parameters depended on the bead size. Furthermore, if the bead edge was weak, image processing was hampered by cluttered edge maps.

The clutter was removed by manually fitting an ellipsoid to the bead outline in the first image. This ellipsoid was then used to create an ellipsoidal filter which was used to remove edge clutter. Since the bead size changes slowly, the filter for the next image was created from the ellipsoid fitted in the previous image. For given set of Canny parameters this procedure proved to be sufficiently robust so that only occasional updates of Canny parameters were required.

The reported bead size is the minor axis of the ellipsoid. This choice was made since both upright and small beads appear slightly elongated; which suggests that for both bead states the shorter length scale is equivalent.

Saturated bead sizes were determined after the experiments by swelling the beads under water for at least 24 h. Bead sizes were then determined by manually fitting ellipses to photos taken with a Nikon D5500.

2. Additional time resolved datasets used to compile steady state data

In this section, we briefly introduce the datasets used to compile the steady state data (figure 10) together with the data presented as figure 3. The three datasets, presented as figures I, II and III, exhibit essentially the same characteristics as the data shown in figure 2 in the main text. The data in figure 2 is the least problematic experiment we conducted and is therefore best suited to introduce these characteristics in a clear fashion. However, it used beads which had previously been used in a different experiment which raises questions about the direct compatibility with other experiments. This is reflected in the fact that for a given hydraulic head the typical bead sizes are considerably larger than in all other experiments we conducted.

The layout of the diagrams and the legend to the curves is analogous to the presentation in the main text, with subfigure (a) showing the bead size, (b) the measured relative humidity and purge flow rate and (c) the derived evaporation rates.

As described in the main text, steady state data was extracted from the datasets by fitting an exponential (main text (2.1)) to $d/d_0(t)$ after an adjustment of the relative humidity was made. When the resultant transition was between two steady states, the characteristic time scale of that change is shown under than transition. We therefore comment only briefly on the particularities of each dataset.

	Beads	d_0 [cm]	$H \pm 0.1$ [cm]	Upright	symbol	Comments
D	2	13.0 12.9	5.2	no	lozenge	only two of four beads reached first steady state.
E	3	12.7 13.1 13.7	10	yes	triangle	
F	4	13.7 13.5 15.1 14.7	20	yes	plus	

Table iii: Overview of the full data sets included in the supplementary material.

We also highlight that the different adjustment of q, depending on whether the relative humidity is increased or decreased, is visible in these datasets for many transitions.

Note that the datasets in figures I to III exhibit slight daily fluctuations in the humidity curves (see e.g. the period between day 11 and 15), which we could eventually attribute to mild temperature fluctuations caused by the discontinuous operation of the heating system of the laboratory.

Figure I shows Dataset D with $H = 5.2\,\mathrm{cm}$. Only two beads remained sealed after two days of evaporation at 43 %. The first relative humidity change was initiated prematurely, e.g., without a steady state having been reached, after two days. Steady states were extracted from this dataset after 6, 10, 14, 16 and 20 days. The dataset shown in figure II shows the dataset from which we obtained the steady state data for $H = 10\,\mathrm{cm}$. Only three beads reached the first steady state after approximately four days. After eight days (bead size spike in figure II), unexpected salt precipitation causing blockage in the humidity adjustment bubblers required a premature change in relative humidity. Steady state data was extracted after approximately 6, 8, 11, 14, 22, 25, 28 and 31 d.

Figure III shows the data used to extract the bead sizes with $H = 20\,\mathrm{cm}$. The data shown was affected by three data logger failures (regions around 5 d, 15 d and 22.5 d). We are confident to extended our fits for steady state data over these gaps as they do not occur during periods where we expected the system to undergo large changes. Steady state data was extracted after approximately 6, 12, 15, and 25 d. The experiment was terminated when after approximately 27 d one bead (black line) started to dry out. Note that the the transition time at approximately 12 d was affected by a brief reduction in purge flow rate caused by salt precipitation in the humidity control system.

2.1. *Steady state table*

In table iv we provide a complete overview of the steady state data and time scales of changes extracted from the experimental data. The index i for each dataset refers to period i marked with arrows in figures 2, 3, 4 and the figures included in the Supplementary Material.

Fig.	DS.	i	$\mathcal{RH}_i$[%] (beg)	(end)	$q[10^{-8}\,\mathrm{m\,s^{-1}}]$ (beg)	(end)	d/d_0 (beg)	(end)	τ_e[d] τ_e
2	A	0	n/a	72	n/a	1.62	n/a	0.71±3.86 %	n/a
2	A	1	72	42	1.62	6.02	0.72±4.00 %	0.48±5.74 %	1.26±3.72 %
2	A	2	42	71	6.02	1.68	0.50±4.04 %	0.71±2.59 %	1.40±2.78 %
2	A	3	71	42	1.68	6.34	0.71±4.19 %	0.48±6.30 %	1.16±3.39 %
2	A	4	42	54	6.34	4.21	0.48±3.61 %	0.55±2.99 %	1.10±7.10 %
2	A	5	54	42	4.21	6.65	0.54±4.26 %	0.46±4.96 %	1.35±44.59 %
2	A	6	42	23	6.65	12.73	0.46±5.05 %	0.29±12.17 %	1.64±34.66 %
3	B	0	n/a	40	n/a	2.73	n/a	0.50±1.68 %	n/a
3	B	1	40	41	2.73	3.47	0.50±1.90 %	0.46±1.82 %	0.73±25.99 %
3	B	2	41	41	3.47	4.21	0.46±3.32 %	0.44±3.83 %	0.57±34.15 %
3	B	3	41	41	4.21	12.96	0.44±2.36 %	0.27±3.32 %	0.22±6.19 %
3	B	4	41	40	12.96	8.53	0.27±2.28 %	0.31±1.96 %	0.22±8.36 %
3	B	5	40	65	8.53	2.78	0.31±1.90 %	0.48±0.75 %	0.67±9.71 %
3	B	6	65	67	2.78	3.75	0.48±2.05 %	0.44±2.12 %	0.83±17.01 %
3	B	7	67	67	3.75	6.28	0.44±2.10 %	0.39±2.41 %	0.51±17.19 %
3	B	8	67	67	8.05	3.57	0.36±1.81 %	0.44±1.75 %	0.56±9.72 %
3	B	9	67	68	3.57	8.06	0.44±3.01 %	0.38±2.29 %	0.47±20.48 %
4	C	0	n/a	45	n/a	5.09	n/a	0.40	n/a
4	C	1	45	45	5.09	6.37	0.40	0.28	0.38
4	C	2	45	45	6.37	7.54	0.28	0.25	0.35
I	D	0	n/a	69	n/a	1.74	n/a	0.59±0.18 %	n/a
I	D	1	69	44	1.74	5.37	0.59±0.69 %	0.40±0.27 %	0.76±6.60 %
I	D	2	44	51	5.37	3.62	0.40±0.60 %	0.44±2.05 %	0.51±0.41 %
I	D	3	51	60	3.62	2.39	0.44±0.48 %	0.48±0.74 %	0.67±22.92 %
I	D	4	60	52	2.39	3.19	0.46±0.97 %	0.43±1.18 %	0.27±31.21 %
II	E	0	n/a	67	n/a	1.72	n/a	0.42±1.34 %	n/a
II	E	1	67	42	1.72	6.12	0.43±1.42 %	0.29±1.98 %	0.57±1.79 %
II	E	2	42	50	6.12	4.69	0.36±2.27 %	0.32±0.87 %	n/a
II	E	3	50	43	4.69	6.48	0.31±1.54 %	0.27±2.32 %	1.13±12.04 %
II	E	4	43	77	6.48	1.28	0.28±1.14 %	0.46±0.85 %	0.81±8.29 %
II	E	5	77	61	1.28	3.26	0.45±1.14 %	0.32±1.38 %	0.68±10.14 %
II	E	6	61	44	3.26	7.01	0.32±0.99 %	0.26±1.27 %	0.30±11.46 %
II	E	7	44	71	7.01	1.80	0.26±1.25 %	0.37±0.84 %	0.42±7.09 %
III	F	0	n/a	44	n/a	6.33	n/a	0.24±8.00 %	n/a
III	F	1	44	75	6.33	1.35	0.28±7.42 %	0.46±4.08 %	1.17±12.26 %
III	F	2	75	62	1.35	3.22	0.48±6.18 %	0.30±11.62 %	1.03±7.28 %
III	F	3	62	72	3.22	1.70	0.28±5.82 %	0.35±4.70 %	0.64±11.40 %

Table iv: Overview of the parameters characterising each transition between steady states. For each transition, we give the inflow relative humidity as measured, q, d/d_0 before and after the transition as well as the characteristic time scale of the transition τ. If applicable, the standard deviation for the set of beads is given in percent. If no transition time is given, the initial state was not a steady state. Arabic figure numbers refer to the main text and roman figure numbers to the Supplementary Material.

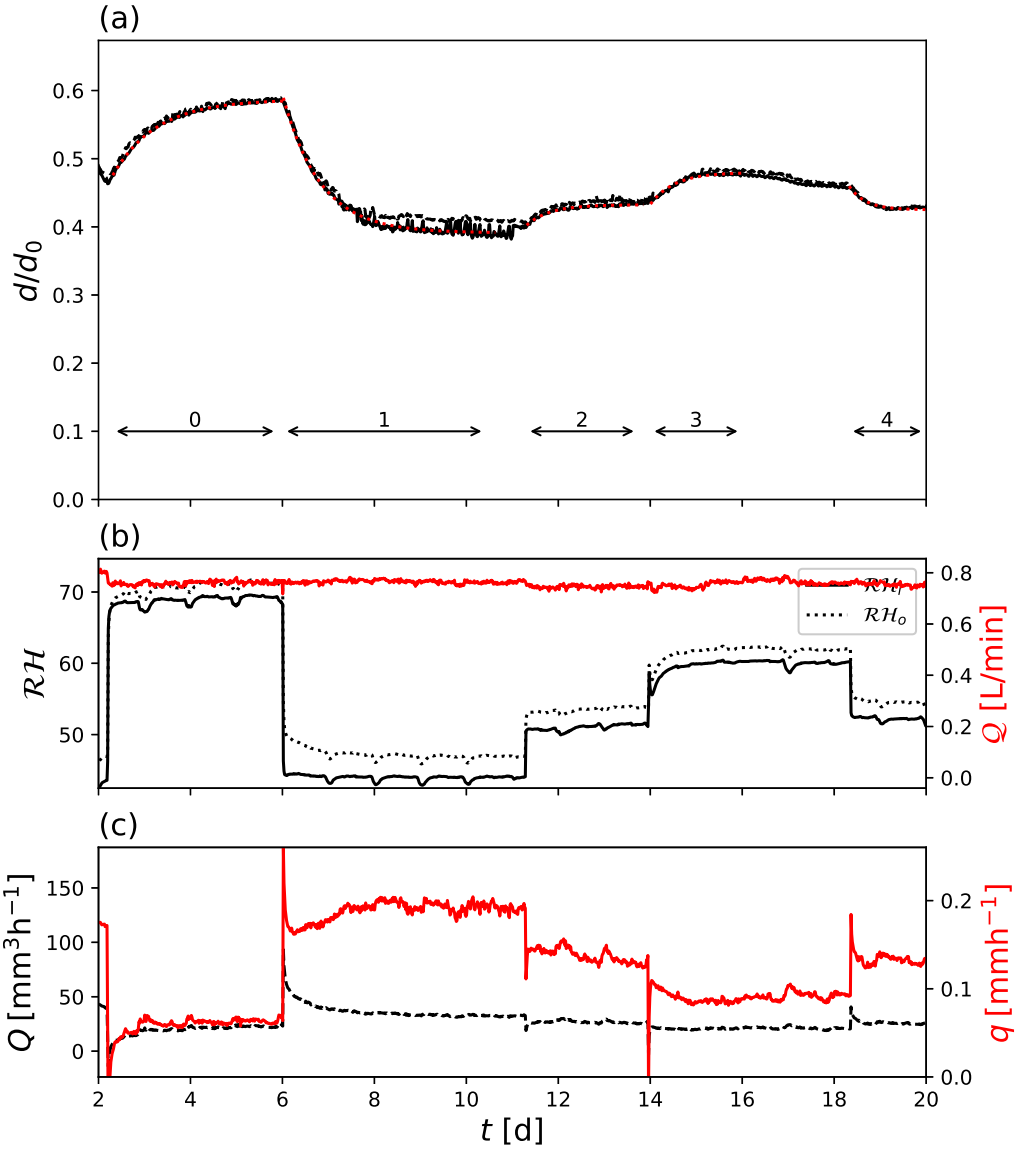

Figure I: Dataset obtained for $H = 5.2\,\mathrm{cm}$ with two beads.

REFERENCES

Greenspan, L. 1977 Humidity fixed points of binary saturated aequeous solutions. *JOURNAL OF RESEARCH of the National Buereou of Standards A* **81A** (1), 89.

MacMinn, Christopher W., Dufresne, Eric R. & Wettlaufer, John S. 2015 Fluid-driven deformation of a soft granular material. *Phys. Rev. X* **5**, 011020.

van der Walt, Stéfan, Schönberger, Johannes L., Nunez-Iglesias, Juan, Boulogne, François, Warner, Joshua D., Yager, Neil, Gouillart, Emmanuelle & Yu, Tony and 2014 scikit-image: image processing in python. *PeerJ* **2**, e453.

Zhang, Yansheng, Etzold, Merlin A & Lefauve, Adrien 2021 Growth of gas-filled penny-shaped cracks in decompressed hydrogels. *Soft Matter* **17** (4), 815–825.

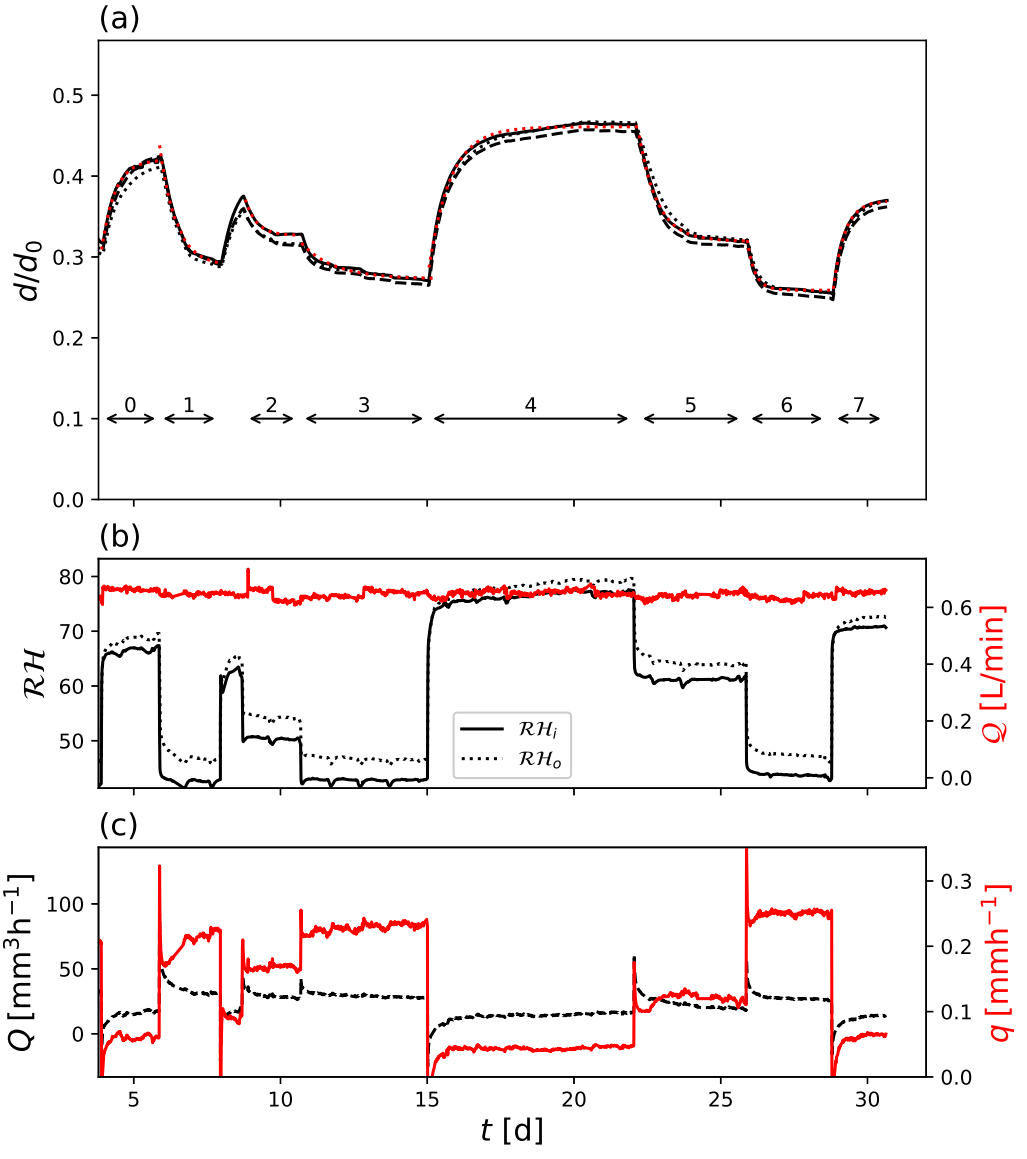

Figure II: Dataset obtained for $H = 10\,\text{cm}$ with three beads.

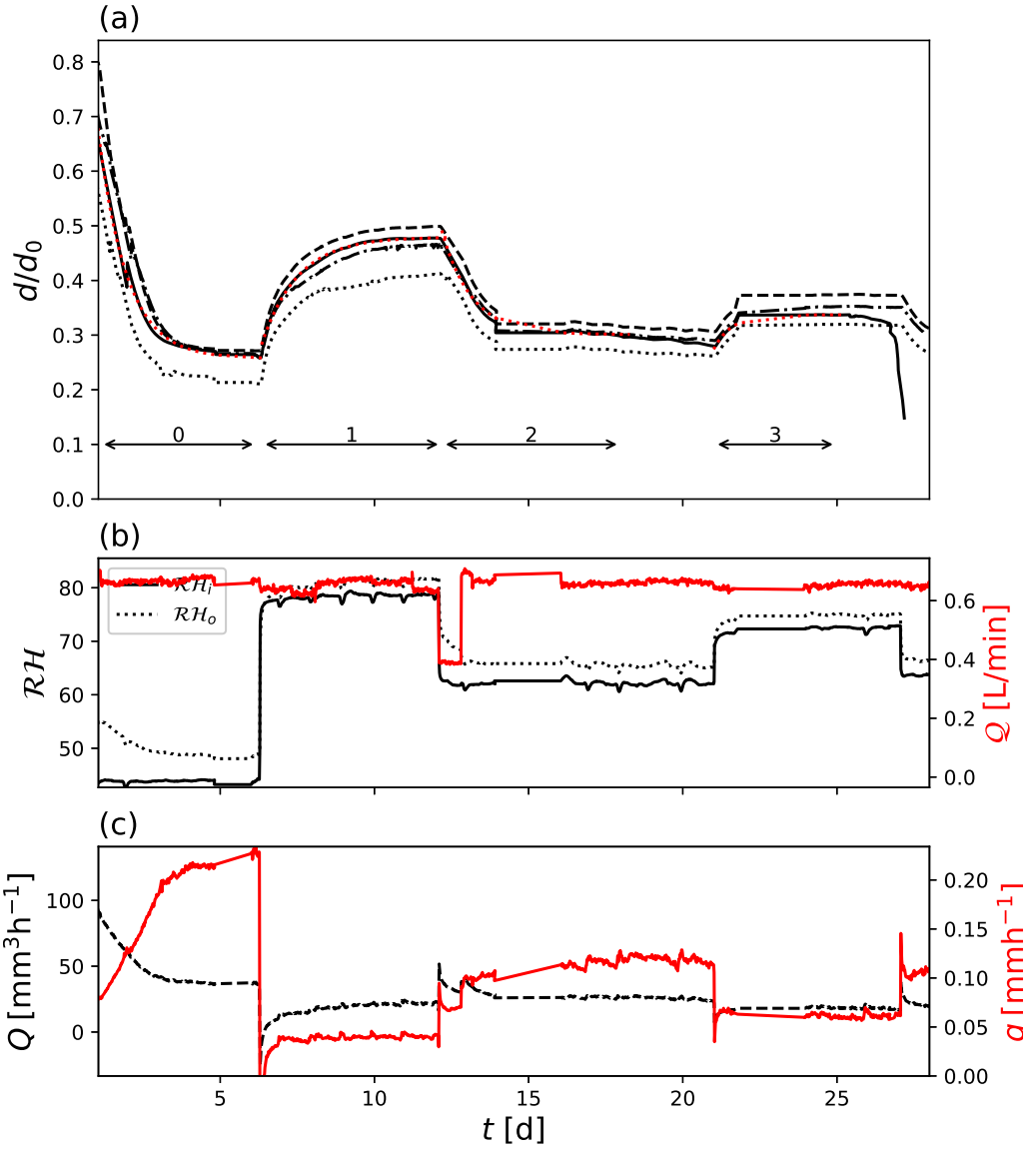

Figure III: Dataset obtained for $H = 20\,\mathrm{cm}$ with four beads.